Heliyon 8 (2022) e10022

Contents lists available at ScienceDirect

Heliyon

journal homepage: www.cell.com/heliyon

Research article

Poly(acrylic acid)/Fe_3O_4 supported on MIL-100(Cr) MOF as a novel and magnetic nanocatalyst for the synthesis of Pyrido[2,3-d]Pyrimidines

Mohammad Ali Ghasemzadeh *, Boshra Mirhosseini-Eshkevari

Department of Chemistry, Qom Branch, Islamic Azad University, Post Box: 37491-13191, Qom, Iran

ARTICLE INFO

Keywords:
Pyrido[2,3-d]Pyrimidines
Metal-organic frameworks
Multi-component reactions
Magnetic nanocomposite
Heterogeneous catalyst

ABSTRACT

In the current work, a convenient and simple approach for preparing poly (acrylic acid)/Fe_3O_4 supported on MIL-100(Cr) for the synthesis of pyrido [2,3-d]pyrimidine derivatives via the three-component one-pot reaction of 1,3-indandione, 6-amino uracil, and aromatic aldehydes is reported. The effectiveness of this new magnetic nanocatalyst was proved. The results showed this nanocatalyst's moderate to high yield under reflux conditions. SEM, TEM, IR, EDX, XRD, BET, and TGA were used to characterize the structure of the synthesized nanocatalyst. This synthetic protocol offers various advantages, including cost-saving, excellent yields in short reaction times (67–98%), low catalyst loading, and catalyst reusability.

1. Introduction

Metal-organic frameworks (MOFs) as a unique class of porous materials, are used as catalysts, heavy-metal adsorption, and gas storage and separation [1, 2, 3, 4]. MOFs present various properties depending on the type of their ligands and their surface functional groups. Functional groups in these frameworks could be firstly available in organic ligand structures, or functional groups could be created within the MOFs structure after their synthesis [5]. To obtain the following objectives, Cr-based MOFs should have improved adsorption, water, thermal stability, and larger surface area in the reaction processes [6, 7].

Multicomponent reactions (MCRs) and related one-pot synthesis (such as tandem, cascade, and domino reactions) are vital in developing novel methodologies in organic catalysis and synthesis because of their countless applications, especially in pharmaceutical works [8, 9, 10, 11, 12, 13]. Hence, complex purification phases are avoided, and time and reagents and solvents are saved [14, 15]. Pyrimidine cores, as main categories of heterocyclic and bioactive molecules, have been recently the subject of intense research in pharmaceutical studies. This great attention is attributed to their broad pharmacological and therapeutic properties, including anti-inflammatory [16], anticancer [17], antimicrobial [18], or antihistaminic activities [19].

One of these materials is pyrido [2,3-d] pyrimidine. This compound is considered an important group of heterocyclic compounds annulated uracil because of their various medicinal applications, like anticonvulsants, antibacterials, and anti-aggressive activities, antileishmanial, antifolate, anti-inflammatory, antimicrobial, and inhibition of cyclin-dependent kinases [20, 21].

We review the studies on synthetic approaches to produce these compounds in the following. Shi et al. (2008) presented pyrimidine derivative synthesis in ionic liquid [bmim]Br, and they obtained 75–93% of yields [22]. Khurana et al. (2012) reported an approach for synthesizing these systems. They used 20 mol% $InCl_3$ (20 mol%) as a catalyst in water and gained 87–90% of product yields [23]. We recently presented various synthesis methods for many products that utilize nanocatalysts [24, 25, 26, 27, 28]. The current work presents a simple method for fabricating Poly (acrylic acid)/Fe_3O_4 Supported on MIL-100(Cr) (Fe_3O_4@PAA@MIL-100(Cr)) as an efficient and robust catalyst. It is an environmentally benign, highly reusable, and heterogeneous catalyst with high catalytic activity for synthesizing pyrido [2,3-d]pyrimidine derivatives through a one-pot three-component condensation reaction of aromatic aldehydes, 1,3-indandione, and 6-amino uracil in EtOH under reflux conditions (Scheme 1).

2. Experimental

2.1. Preparation of Fe_3O_4-PAA

Fe_3O_4@PAA nanocomposite was prepared according to a method reported by Tian Jin *et al* [29]. Typically, we added 0.6 g PAA to a mix of 0.75 g $FeCl_3.6H_2O$ in 40 mL ethylene glycol, followed by stirring the solution at ambient temperature for 30 min. Afterward, NaOAc (2.5 g)

* Corresponding author.
E-mail address: ghasemzadeh@qom-iau.ac.ir (M.A. Ghasemzadeh).

https://doi.org/10.1016/j.heliyon.2022.e10022
Received 27 March 2022; Received in revised form 27 May 2022; Accepted 18 July 2022

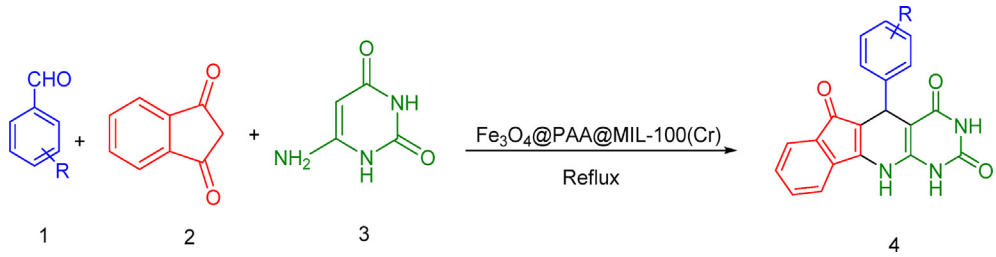

Scheme 1. Synthesis of pyrido [2,3-d]pyrimidines using Fe_3O_4@PAA@MIL-100(Cr).

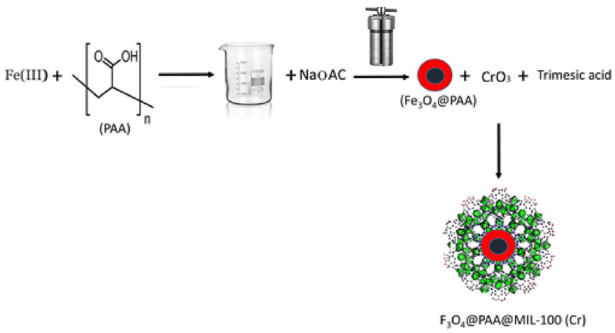

Scheme 2. Preparation of Fe_3O_4@PAA@MIL-100(Cr).

was added to the solution and it was placed in a 50 mL Teflon-lined stainless steel autoclave at of 200 °C for 24 h. Then, the resulting residue was rinsed three times using ethanol and deionized water and dispersed in ethanol (40 mL).

2.2. Synthesis of Fe_3O_4@PAA@MIL-100(Cr)

Briefly, trimesic acid (1.05 g) and CrO_3 (0.5 g) were dissolved in H_2O (2 mL) and HF (0.2 g). In the next step, it was mixed with an as-prepared Fe_3O_4@PAA solution (10 mL). The obtained solution was stirred for 2 h at 80 °C. Lastly, the synthesized Fe_3O_4@PAA@MIL-100(Cr) was rinsed using ethanol, and dried at 100 °C (Scheme 2).

2.3. General procedure for the synthesis of indeno [2′,1′:5,6]pyrido [2,3-d]pyrimidines (4a-p) using Fe_3O_4@PAA@MIL-100(Cr) nanocatalyst

The mixture of Fe_3O_4@PAA@MIL-100(Cr) (0.008 g), 1,3-indandione (1 mmol), aromatic aldehyde (1 mmol), and 6-amino uracil (1 mmol) in ethanol (5 mL) was refluxed for 30 min. The mixture was cooled to room temperature when the reaction (which was TLC-monitored) was completed, and the resulting solid was subsequently dissolved in dichloromethane. A straightforward filtering was used to isolate the catalyst, which was insoluble in CH_2Cl_2. M. p., FT-IR, ^{1}H NMR and ^{13}C NMR spectroscopy methods were performed to characterize and identify of all the products.

The spectral data of some products are provided, as below.

5-(4-chlorophenyl)-5,11-dihydro-1H-indeno [2′,1′:5,6] pyrido [2,3-d] pyrimidine-2,4,6-trione (4d): Yellow solid; m. p. >300 °C °C. IR spectrum ν, cm^{-1}: 3362, 3285, 3073, 2815, 1714, 1646, 1633, 1544, 1511, 1023, ^{1}H NMR (250 MHz, DMSO-d_6) δ: 4.74 (s, 1H, CH),7.12 (d, 2H, J = 8.1 Hz, Ar–H), 7.25 (d, 2H, J = 8.2 Hz, Ar–H), 7.46–7.49 (m, 4H, Ar–H), 8.45 (s, br. 1H, NH), 10.28 (s, br. 1H, NH), 10.84 (s, br. 1H, NH); ^{13}C NMR (62.9 MHz, DMSO-d_6) δ: 38.5, 78.6, 104.5, 123.2, 124.5, 126.3, 127.8, 128.5, 128.9, 133.3, 135.4, 136.7, 144.5, 145.8, 153.4, 161.6,

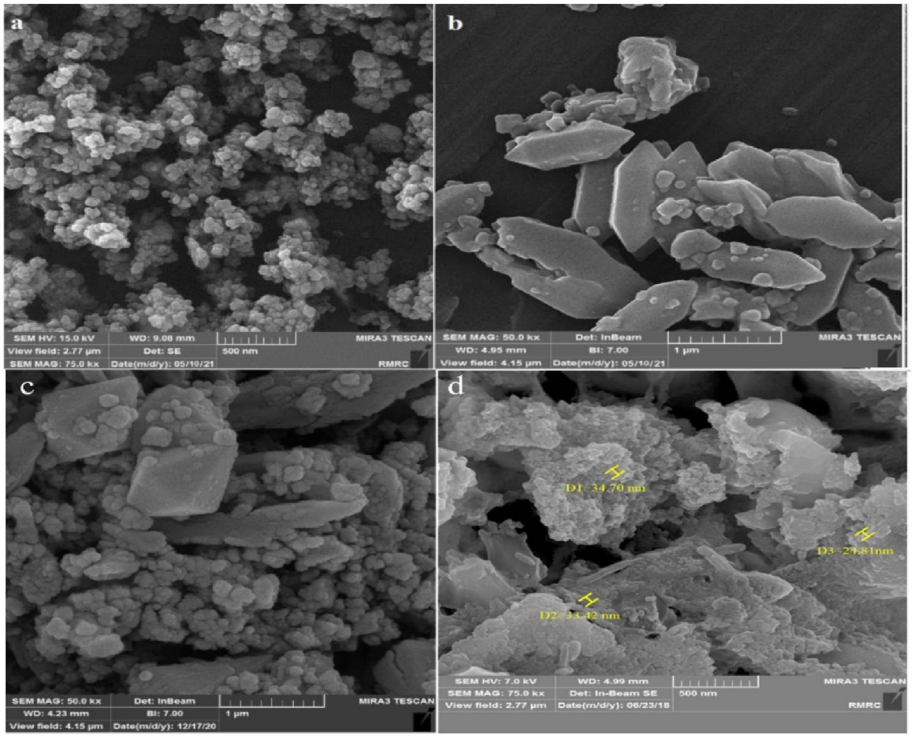

Figure 1. FE-SEM images of Fe_3O_4 (a), MIL-100(Cr) (b), Fe_3O_4@PAA (c), and Fe_3O_4@PAA@MIL-100(Cr) (d).

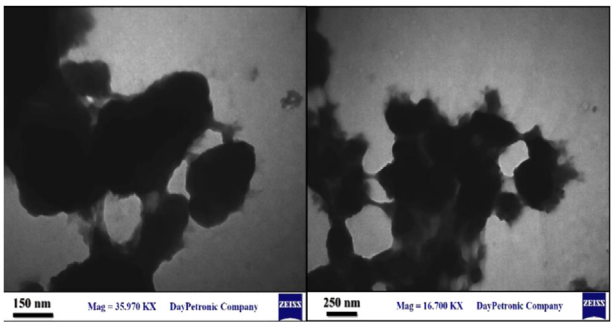

Figure 2. TEM images of Fe_3O_4@PAA@MIL-100(Cr).

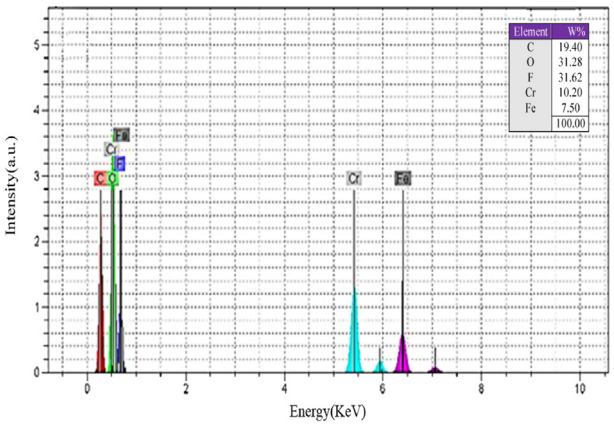

Figure 3. The EDX spectrum of Fe_3O_4@PAA@MIL-100(Cr).

163.5, 191.4; Anal. Calcd. for $C_{20}H_{12}ClN_3O_3$: C 63.59, H 3.20, N 11.12. Found: C, 63.54, H 3.17, N 11.09; MS (EI) (m/z): 377.06 (M^+).

5-(4-methylphenyl)-5,11-dihydro-1H-indeno [2′,1′:5,6] pyrido [2,3-d] pyrimidine-2,4,6-trione (4e): Yellow solid; m. p. >300 °C °C. IR spectrum ν, cm^{-1}: 3365, 3276, 3078, 2811, 1709, 1653, 1632, 1546, 1516, 1025, ^{1}H NMR (250 MHz, DMSO-d_6) δ: 2.25 (s, 3H, CH_3), 4.76 (s, 1H, CH), 7.08 (d, 2H, J = 8.2 Hz, Ar–H), 7.26 (d, 2H, J = 8.1 Hz, Ar–H), 7.55–7.59 (m, 4H, Ar–H), 8.49 (s, 1H, NH), 10.35 (s, 1H, NH), 10.82 (s, 1H, NH); ^{13}C NMR (62.9 MHz, DMSO-d_6) δ: 17.8. 39.3, 78.7, 105.9, 123.6, 125.8, 126.3, 127.2, 128.1, 128.3, 132.1, 135.3, 136.5, 144.1, 146.7, 152.7, 162.8, 164.5, 193.1; Anal. Calcd. for $C_{21}H_{15}N_3O_3$: C 70.58, H 4.23, N 11.76. Found: C, 70.54, H 4.21, N 11.74; MS (EI) (m/z): 357.11 (M^+).

5-(4-fluorophenyl)-5,11-dihydro-1H-indeno [2′,1′:5,6] pyrido [2,3-d] pyrimidine-2,4,6-trione (4f): Yellow solid; m. p. >300 °C °C. IR spectrum ν, cm^{-1}: 3364, 3283, 3072, 2814, 1715, 1643, 1635, 1546, 1513, 1024, ^{1}H NMR (250 MHz, DMSO-d_6) δ: 4.75 (s, 1H, CH),7.16 (d, 2H, J = 8.2 Hz, Ar–H), 7.23 (d, 2H, J = 8.4 Hz, Ar–H), 7.43–7.46 (m, 4H, Ar–H), 9.04 (s, br. 1H, NH), 10.65 (s, br. 1H, NH), 10.94 (s, br. 1H, NH); ^{13}C NMR (62.9 MHz, DMSO-d_6) δ: 39.5, 79.6, 102.5, 123.3, 125.5, 126.2, 127.1, 128.4, 128.7, 133.2, 135.2, 136.8, 144.2, 146.5, 153.2 ($^1J_{C\text{-}F}$ = 158 Hz), 161.4, 163.2, 191.5; Anal. Calcd. for $C_{20}H_{12}FN_3O_3$: C 66.48, H 3.35, N 11.63. Found: C, 66.45, H 3.38, N 11.65; MS (EI) (m/z): 361.09 (M^+).

5-(2-fluorophenyl)-5,11-dihydro-1H-indeno [2′,1′:5,6] pyrido [2,3-d] pyrimidine-2,4,6-trione (4n): Yellow solid; m. p. >300 °C °C. IR spectrum ν, cm^{-1}: 3368, 3288, 3077, 2811, 1714, 1641, 1633, 1543, 1512, 1021, ^{1}H NMR (250 MHz, DMSO-d_6) δ: 4.77 (s, 1H, CH),7.17 (d, 2H, J = 8.6 Hz, Ar–H), 7.26 (d, 2H, J = 8.2 Hz, Ar–H), 7.41–7.43 (m, 4H, Ar–H), 9.08 (s, br. 1H, NH), 10.69 (s, br. 1H, NH), 10.91 (s, br. 1H, NH); ^{13}C NMR (62.9 MHz, DMSO-d_6) δ: 39.6, 79.5, 102.7, 123.8, 125.1, 126.4, 127.2, 128.3, 128.8, 133.1, 135.5, 136.7, 144.6, 146.7, 153.5, 161.3 ($^1J_{C\text{-}F}$ = 148 Hz), 163.5, 191.4; Anal. Calcd. for $C_{20}H_{12}FN_3O_3$: C 66.48, H 3.35, N 11.63. Found: C, 66.46, H 3.37, N 11.66; MS (EI) (m/z): 361.09 (M^+).

4-(2,4,6-trioxo-2,3,4,5,6,11-hexahydro-1H-indeno [2′,1':5,6] pyrido [2,3-d] pyrimidin-5-yl)benzonitrile (4o): Yellow solid; m. p. >300 °C. IR spectrum ν, cm^{-1}: 3365, 3172, 3051, 2932, 1705,1674, 1591, 1458, 1205; ^{1}H NMR (250 MHz, DMSO-d_6) δ: 4.33 (s, 1H, CH), 6.74–7.05 (d, 2H, J = 8.6 Hz, ArH), 7.28–7.32 (d, 2H, J = 8.3 Hz, ArH), 7.62–7.78 (m, 4H, ArH), 9.45 (s, 1H, NH), 10.12 (s, 1H, NH), 10.50 (s, 1H, NH); ^{13}C NMR (62.9 MHz, DMSO-d_6) δ: 27.33, 31.39, 68.62, 76.82, 87.26, 101.03, 112.53, 123.45, 131.34, 133.43, 134.25, 138.56, 144.43, 146.33, 148.62, 156.47, 165.38, 168.28, 170.21, 183.31, 188.22; Anal. Calcd. for $C_{21}H_{12}N_4O_3$: C 68.48, H 3.28, N 15.21; Found: C, 68.46, H 3.25, N 15.18; MS (EI) (m/z): 368.35 (M^+).

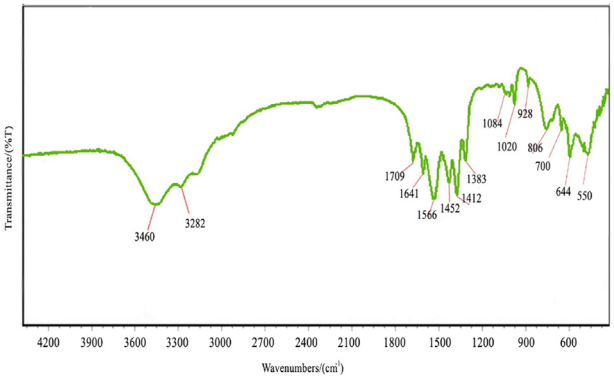

Figure 4. FT-IR spectrum of Fe_3O_4@PAA@MIL-100(Cr).

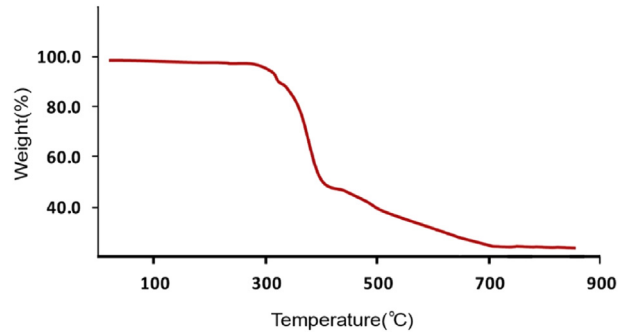

Figure 5. TGA curve of Fe_3O_4@PAA@MIL-100(Cr).

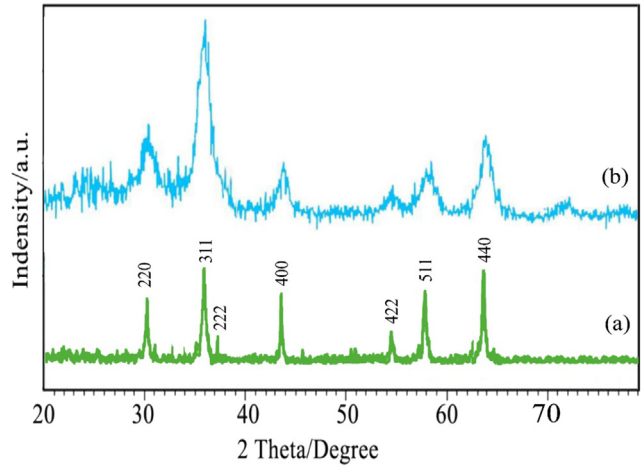

Figure 6. XRD patterns of Fe_3O_4 (a), and Fe_3O_4@PAA@MIl-100(Cr) (b).

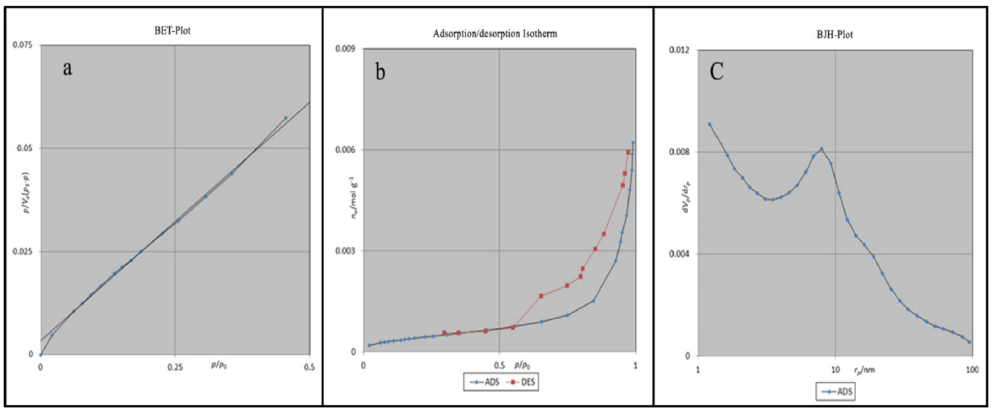

Figure 7. BET-plot of Fe_3O_4@PAA@MIL-100(Cr) (a), adsorption/desorption of Fe_3O_4@PAA@MIL-100(Cr) (b), and BJH-plot of Fe_3O_4@PAA@MIL-100(Cr) (c).

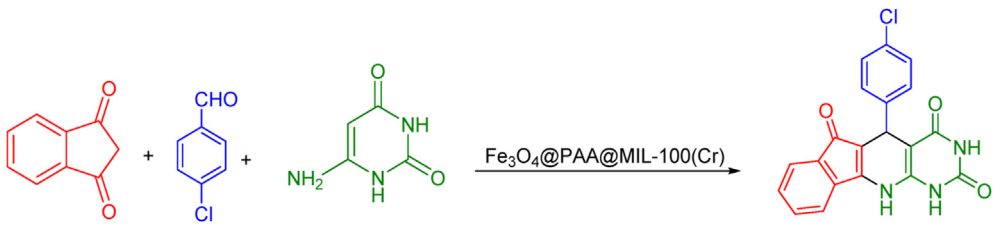

Scheme 3. The model reaction for the synthesis of pyrido [2,3-d]pyrimidine **4d**.

5-(4-(methylthio)phenyl)-5,11-dihydro-1H-indeno [2′,1':5,6] pyrido [2,3-d] pyrimidine-2,4,6(3H)-trione (4p): Yellow solid; m. p. >300 °C. IR spectrum ν, cm^{-1}: 3365, 3172, 3051, 1705, 1674, 1591, 1500, 1485, 1375, 1205; ^{1}H NMR (250 MHz, DMSO-d_6) δ: 2.73 (s, 3H, CH_3), 4.64 (s, 1H, CH), 6.76–7.04 (d, 2H, J = 8.2 Hz, ArH), 7.28–7.36 (d, 2H, J = 8.3 Hz, ArH), 7.65–7.77 (m, 4H, ArH), 9.85 (s, 1H, NH), 10.51 (s, 1H, NH), 10.83 (s, 1H, NH); ^{13}C NMR (62.9 MHz, DMSO-d_6) δ: 28.39, 32.33, 67.62, 77.82, 86.26, 102.03, 113.52, 125.44, 132.34, 134.43, 136.26, 139.56, 146.44, 148.33, 149.69, 154.47, 162.34, 164.28, 171.21, 181.32, 187.21; Anal. Calcd. for $C_{21}H_{15}N_3O_3S$: C 64.77, H 3.88, N 10.79; Found: C, 64.75, H 3.86, N 10.75; MS (EI) (m/z): 389.08 (M^+).

3. Results and discussion

Using EDX, FE-SEM, TEM, FT-IR, BET, TGA, and XRD techniques, the Fe_3O_4@PAA@MIL-100(Cr) nanostructure was studied in the main experiments. A magnetic core with a strong inclination between the ligand and the receptor and through the specific gravity absorption of

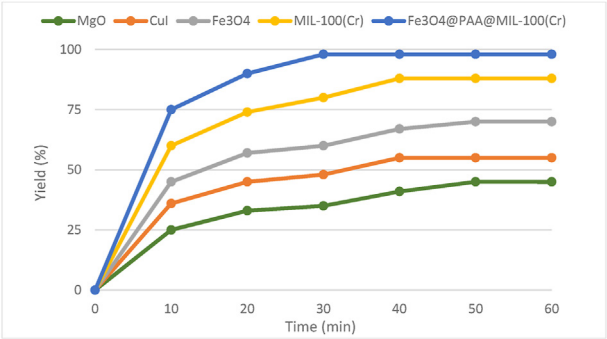

Figure 9. The effect of various catalysts on model reaction.

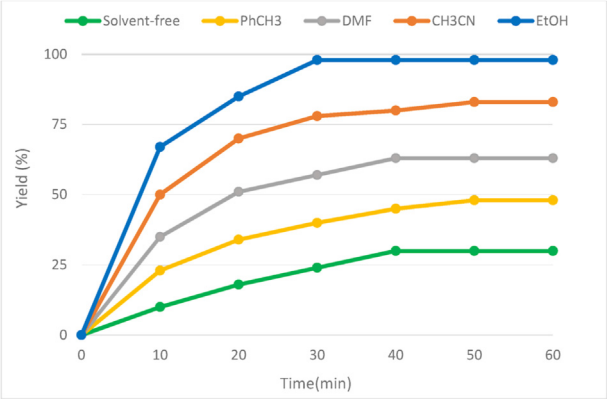

Figure 8. The influence of various solvents in model study.

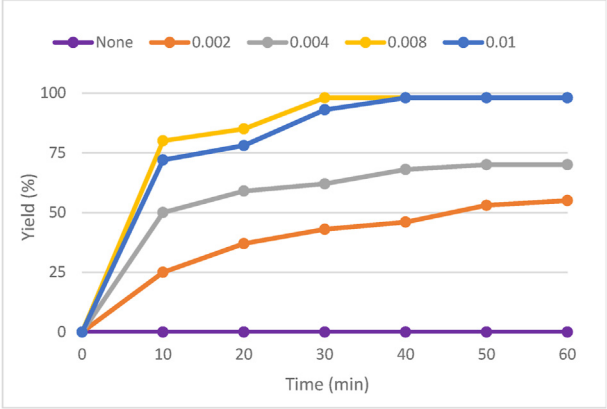

Figure 10. The effect of catalyst amount on the model reaction.

Table 1. Synthesis of pyrido [2,3-d]pyrimidine derivatives using Fe_3O_4@PAA@MIL-100(Cr)

Entry	ArCHO	Product	Time (min)	Yield (%)[a]	M.p. °C	Lit. M.p. °C
1	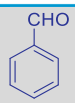	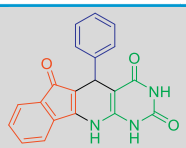 4a	45	76	>300 °C	>300 °C [36]
2	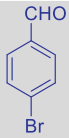	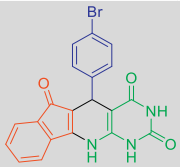 4b	35	95	>300 °C	>300 °C [36]
3	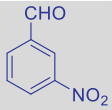	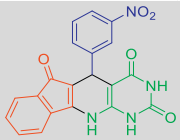 4c	40	87	>300 °C	>300 °C [36]
4	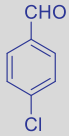	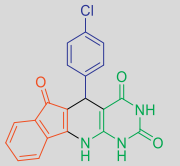 4d	30	98	>300 °C	>300 °C [36]
5	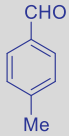	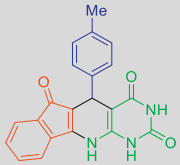 4e	50	75	>300 °C	>300 °C [36]
6	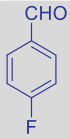	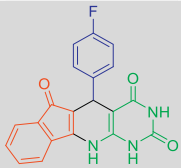 4f	30	94	>300 °C	>300 °C [36]
7	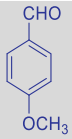	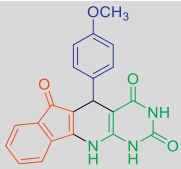 4g	45	78	>300 °C	>300 °C [36]
8	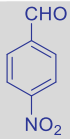	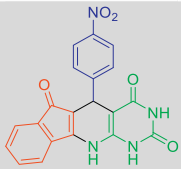 4h	35	96	>300 °C	>300 °C [36]
9		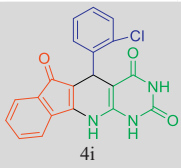 4i	40	80	>300 °C	>300 °C [36]
10			45	79	>300 °C	>300 °C [22]

(*continued on next page*)

Table 1 (*continued*)

Entry	ArCHO	Product	Time (min)	Yield (%)[a]	M.p. °C	Lit. M.p. °C
	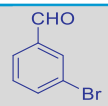	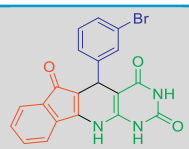 4j				
11	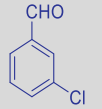	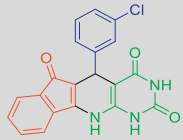 4k	50	83	>300 °C	>300 °C [22]
12	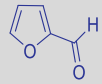	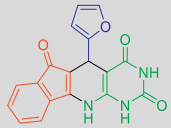 4l	45	67	>300 °C	>300 °C [36]
13	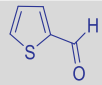	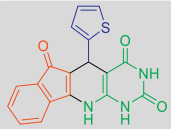 4m	40	63	>300 °C	>300 °C [36]
14		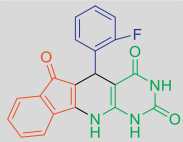 4n	35	85	>300 °C	>300 °C [22]
15	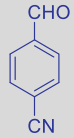	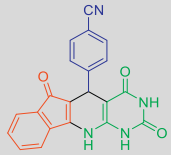 4o	30	92	>300 °C	———[b]
16	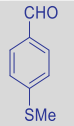	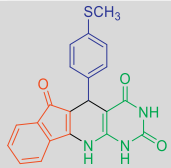 4p	40	86	>300 °C	———[b]

[a] Isolated yield.
[b] New Products.

the tissue is provided by Fe_3O_4 in the generated heterogeneous nanocomposite. Additionally, when placed in an acidic environment, polyacrylic acid acts as a polymer layer between Fe_3O_4 and MOF to conduct Fe_3O_4 magnetic and produce a cleft in the MIL-100(Cr) structure. The polyacrylic acid (PAA) chains in this composite served as a bridge to connect the MIL-100(Cr) layer outside and the magnetite nanoparticles Fe_3O_4 inside.

Scanning electron microscopy was used to visualize the results of the SEM examination for each stage of the catalyst synthesis. This examination appeared that Fe_3O_4 is composed of moderately uniform circular particles (Figure 1a). [30]. According to literature, the SEM image of MIL-100(Cr) showed that this structure has a typical octahedral shape (Figure 1b) [31]. The Fe_3O_4@PAA composite dispersity worsens as a result of the coated PAA ease of coating, as demonstrated by the SEM picture of the Fe_3O_4@PAA in Figure 1c [32]. Because of the connection between MIL-100(Cr) and Fe_3O_4 created by polyacrylic acid, the particles in the SEM image of Fe_3O_4@PAA@MIL-100(Cr) have a cloudy appearance (Figure 1d).

Transmission electron microscopy (TEM) analysis of the Fe_3O_4@PAA@MIL-100(Cr) are shown in Figure 2. The morphology and the topology of the nanocatalyst were confirmed to be cloudy structures. The particles of Fe_3O_4@PAA@MIL-100(Cr) were observed of nano-sized (approximately 25–35 nm) with proper dispersion.

Chemical characterization and structural investigation of the sample were carried out using energy-dispersive X-ray (EDX) spectroscopy as an analytical technique. C, Fe, F, Cr, and O are the only elementary components in Fe_3O_4@PAA@MIL-100(Cr), as shown in the EDX spectrum (Figure 3).

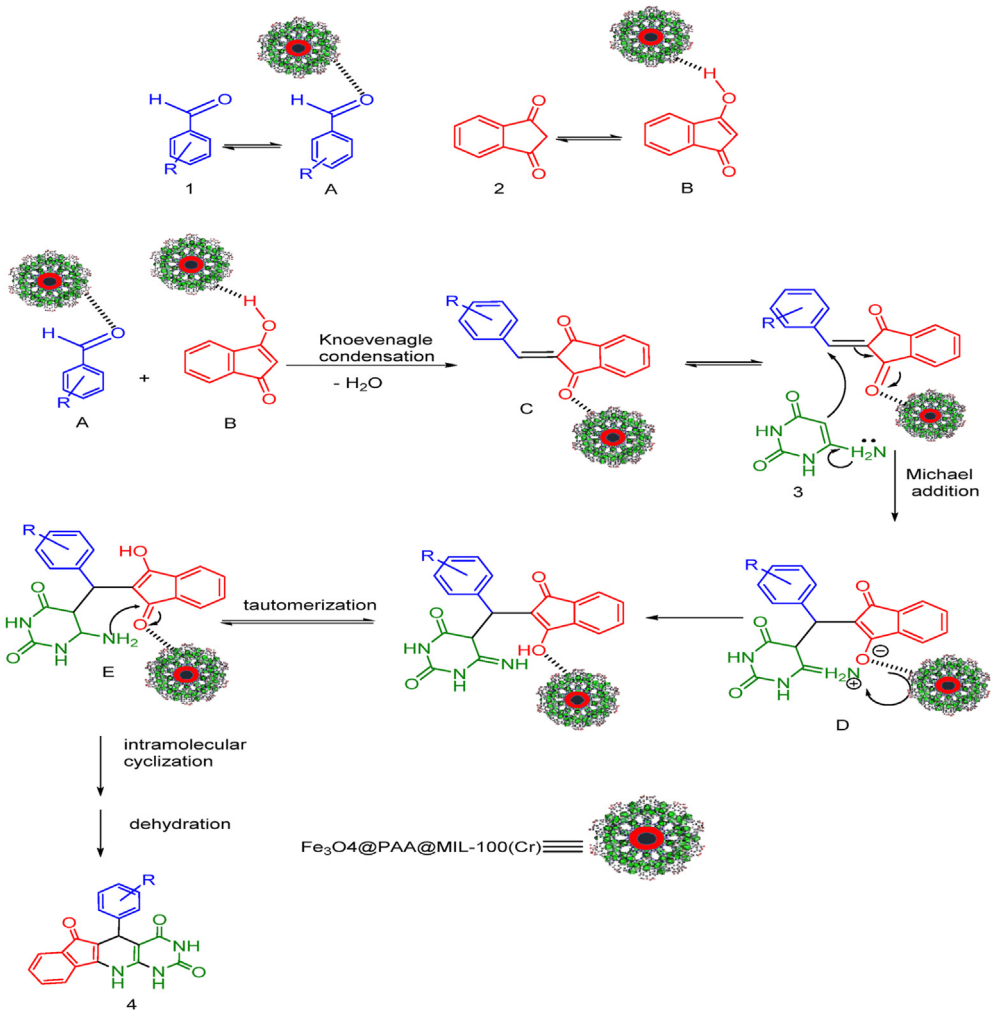

Scheme 4. Proposed reaction mechanism for preparation of pyrido [2,3-d]pyrimidines using Fe_3O_4@PAA@MIL-100(Cr).

Figure 4 represents the FT-IR spectrum of Fe_3O_4@PAA@MIL-100(Cr). The absorption band at 550 cm^{-1} is due to the Fe–O stretching vibration [33]. The peaks in 1412 and 1566 cm^{-1} are due to C–O and C=O stretching vibrations of PAA, respectively. Besides, the stretching vibration of OH groups of PAA was observed at 3460 cm^{-1}. The vibration bands as characteristics of framework (O–C–O) groups appeared near 1709 and 1383 cm^{-1}, confirming the tricarboxylate coordination in the MIL-100(Cr) framework. The peak at 1452 cm^{-1} is attributed to the C=C bond vibration in tricarboxylate rings. Intense bands at about 3282 and 1641 cm^{-1} proved the presence of water molecules in the Fe_3O_4@PAA@MIL-100(Cr) [34].

Thermal gravimetric analysis (TGA) was used to measure the mass reduction caused by heating under a nitrogen gas stream (Figure 5). Fe_3O_4@PAA@MIL-100(Cr) structure depicts two stages of weight loss. At temperatures between 300 and 400 °C, organic molecules from the composite including PAA are destroyed. The second case is in the 400–850 °C range, which is attributed to destructing metal-organic framework (MIL-100(Cr)) in the Fe_3O_4@PAA@MIL-100(Cr) structure.

Table 2. The comparison of the outcomes of the production of pyrido [2,3-d] pyrimidines by means of different catalysts[a].

Entry	Catalyst	Conditions	Time/yield (%)	References
1	[bmim]Br	Solvent-free/95 °C	210 min/ 89-91	[22]
2	$InCl_3$	H_2O/Reflux	60 min/87-90	[23]
3	[DMBSI]HSO_4	Ethylene glyco 1/ Reflux	4h/87-95	[36]
4	Nano-Fe_3O_4@SiO_2–SO_3H	H_2O/Stir. (70 °C)	25 min/90-94	[37]
5	Nano-Fe_3O_4@cellulose-SO_3H	H_2O/Stir.80 °C	30 min/85-95	[38]
6	**Fe_3O_4@PAA@MIL-100(Cr)**	**EtOH/Reflux**	**30 min/75-98**	**This work**

[a] Based on the three-component reaction of 4-chlorobenzaldehyde, 1,3-indandione, and 6-amino uracil.

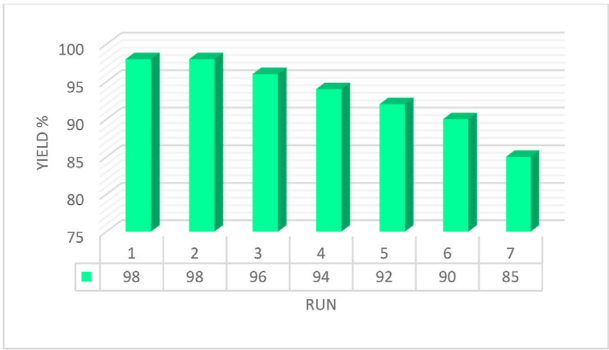

Figure 11. Reusability of the Fe_3O_4@PAA@MIL-100(Cr) catalyst.

To determine the crystaline structure of the nanocomposite, X-ray diffraction pattern (XRD) was used. Figure 6 displays the XRD patterns for Fe_3O_4 nanoparticles and Fe_3O_4@PAA@MIL-100(Cr). The indices of the typical peaks for Fe_3O_4 are (220) (311) (222) (400) (422) (511) and (440). All of the peaks locations and relative intensities match up well with the Fe_3O_4 with P63mc group standard XRD pattern (JCDPS No. 75–0449), demonstrating that the crystalline cubic spinel was retained during the functionalization of MNPs [35]. Figure 6b indicates the diffraction peaks for Fe_3O_4@PAA@MIl-100(Cr), confirming the Fe_3O_4 crystallinity following functionalization with MIL-100(Cr) and polyacrylic acid.

Nitrogen adsorption using the BET technique was applied to determine the surface area of the Fe_3O_4@PAA@MIl-100(Cr). As shown by BET analysis for Fe_3O_4@PAA@MIL-100(Cr), the available surface area was 1248 m^2 g^{-1}. The cavity volume in the Fe_3O_4@PAA@MIL-100(Cr) was 0.8112 cm^3gr^{-1} (Figure 7a). Figure 7b indicates the desorption-adsorption isotherm for Fe_3O_4@PAA@MIL-100(Cr) as a type I sorption isotherm. The average pore diameter of the nanocarrier, as determined by the findings of the BJH study, was 1.23 nm, confirming the presence of porosity in the MOF (Figure 7c).

In continue, the condensation reaction of 4-chlorobenzaldehyde, 1,3-indandione, and 6-amino uracil was chosen as a model study to optimize the reaction and examine the effects of the catalyst, reactants, and solvent on the of synthesis of pyrido [2,3-d]pyrimidine derivatives (Scheme 3).

Initially, the effect of various solvents and solvent-free conditions were examined when we used Fe_3O_4@PAA@MIL-100(Cr) as a catalyst in the preparation of pyrido [2,3-d]pyrimidine 4d. As can be observed, the solvent significantly affects the reaction rate (Figure 8). Ethanol afforded the best results (98% of yield) under reflux conditions for this multi-component reaction.

In continue, the significance of the prepared catalyst in comparison to other catalysts was studied. Existing catalysts such as MgO, CuI, Fe_3O_4, MIL-100(Cr), and Fe_3O_4@PAA@MIL-100(Cr) were all applied under reflux conditions while utilizing ethanol as a solvent. According to Figure 9, Fe_3O_4@PAA@MIL-100(Cr) was the best catalyst regarding the reaction time and obtained product yield.

The study model was discussed in the following using various quantities of Fe_3O_4@PAA@MIL-100(Cr) nanocatalyst. The optimal concentration of Fe_3O_4@PAA@MIL-100(Cr) was found at 0.008 g (Figure 10). As indicated, the reaction duration and yield were not altered by a quantity greater than 0.008 g.

We studied the scope of this research by synthesizing pyrido [2,3-d]pyrimidine derivatives using various aromatic aldehydes comprising electron-donating and electron-withdrawing groups in the presence of 0.008 g of Fe_3O_4@PAA@MIL-100(Cr) nanocomposite. According to Table 1, prolonged reaction time is required by aryl aldehydes with electron-donating groups to afford the corresponding products. However, the aryl aldehydes with withdrawing groups reacted faster to produce pyrido [2,3-d]pyrimidines. According to the mechanism pathway (Scheme 4), the first step of the mechanism is the Knoevenagel condensation between 1,3-indandione and aromatic aldehyde. Obliviously, the presence of electron-withdrawing groups on the benzaldehydes leads to a faster reaction due to more electrophilicity of the carbon group of the carbonyl. While using Fe_3O_4@PAA@MIL-100(Cr) as a catalyst serves as a Lewis acid catalyst and causes to increase in electrophilicity of the carbonyl groups of aldehydes. The synergic effects of both electron-withdrawing groups and Lewis acidity of Fe_3O_4@PAA@MIL-100(Cr) increase the rate of the reaction. However, against the electron-withdrawing groups, the existence of electron-donating groups causes to decrease in the speed of the reaction, because of a slower nucleophilic attack on carbonyl groups of aldehydes.

We compared the usability and efficiency of our catalyst to synthesize pyrido [2,3-d]pyrimidine derivatives and other catalysts reported previously. According to Table 2, Fe_3O_4@PAA@MIL-100(Cr) outperformed other catalysts in saving energy, time, and superior yields of the products (Table 2).

3.1. Reuse of catalyst

The catalyst reusability is well known as the key characteristic feature. Here, we assessed the retrievability of the Fe_3O_4@PAA@MIL-100(Cr) on the reaction of 4-chlorobenzaldehyde 1,3-indandione, and 6-amino uracil. As shown in Figure 11, the catalytic activity of Fe_3O_4@PAA@MIL-100(Cr) reduced from 98% in the fresh run to 85% after 7 runs.

Scheme 4 shows the plausible mechanism to prepare pyrido [2,3-d] pyrimidines in the presence of Fe_3O_4@PAA@MIL-100(Cr) nanostructure as the catalyst. When there are Lewis acidic sites over the catalyst surface, the reactants may undergo reaction within a shorter time. The results were examined experimentally based on the literature [37, 38]. Fe_3O_4 and MIL-101(Cr) are thought to function as Lewis acids that, through a potent coordination bond, boost the electrophilicity of the carbonyl groups of 1,3-indandione and aldehyde [39, 40]. In the first step, it is assumed that, electron pairs of the carbonyl groups of the 1, 3-indandione and aryl aldehydes were interacted with the catalyst to improve the electrophilicity features of the functional groups (formation of intermediates A and B). In addition, the intermediate (C) was obtained via the Knoevenogel condensation between intermediate A and B. Then, by the 6-aminouracil attacks to the intermediate (C), the intermediate (D) formed through the Michael addition. Next, tautomerization of intermediate D led to the formation of intermediate E, by intramolecular cyclization and dehydration to produce 5-aryl-5,11-dihydro-1H-indeno [2′,1′:5,6]pyrido [2,3-d]pyrimidine-2,4,6-trione 4.

4. Conclusio

In summary, we prepared and characterized Fe_3O_4@PAA@MIL-100(Cr) magnetic nano-catalyst as a magnetically recyclable, green and bio-friendly catalyst. This catalyst was applied to synthesize pyrido [2,3-d]pyrimidine derivatives via a three-component reaction of 1,3-indandione, 6-amino uracil, and aromatic aldehydes. By this approach, some benefits including great yields in short reaction time, high atom economy, and mild reaction conditions were provided.

Declarations

Author contribution statement

Mohammad Ali Ghasemzadeh: Conceived and designed the experiments; Analyzed and interpreted the data; Contributed reagents, materials, analysis tools or data; Wrote the paper.

Boshra Mirhosseini-Eshkevari: Performed the experiments; Analyzed and interpreted the data; Contributed reagents, materials, analysis tools or data; Wrote the paper.

Funding statement

This work was supported by the Research Affairs Office of the Islamic Azad University, Qom Branch, Qom, I. R. Iran (grant number 2019-2898).

Data availability statement

Data will be made available on request.

Declaration of interests statement

The authors declare no conflict of interest.

Additional information

No additional information is available for this paper.

References

[1] J.Y. Lee, O.K. Farha, J. Roberts, K.A. Scheidt, S.T. Nguyen, J.T. Hupp, Metal-organic framework materials as catalysts, Chem. Soc. Rev. 38 (2009) 1450–1459.

[2] T.A. Goetjen, X. Zhang, J. Liu, J.T. Hupp, O.K. Farha, Metal-Organic Framework supported single site chromium (III) catalyst for ethylene oligomerization at low pressure and temperature, ACS Sustain. Chem. Eng. 7 (2019) 2553–2557.

[3] C.C. Cao, C.X. Chen, Z.W. Wei, Q.F. Qiu, N.X. Zhu, Y.Y. Xiong, J.J. Jiang, D. Wang, C.Y. Su, Catalysis through dynamic spacer installation of multivariate functionalities in metal-organic frameworks, J. Am. Chem. Soc. 141 (2019) 2589–2593.

[4] E. Nowacka, P. Briantais, C. Prestipino, F.X. Llabrés i Xamena, Selective aerobic oxidation of cumene to cumene hydroperoxide over mono-and bimetallic trimesate metal-organic frameworks prepared by a facile "green" aqueous synthesis, ACS Sustain. Chem. Eng. 7 (2019) 7708–7715.

[5] X.C. Huang, Y.Y. Lin, J.P. Zhang, X.M. Chen, Ligand-directed strategy for zeolite-type metal-organic frameworks: zinc (II) imidazolates with unusual zeolitic topologies, Angew. Chem. Int. Ed. 45 (2006) 1557–1559.

[6] S.H. Jhung, N.A. Khan, Z. Hasan, Analogous porous metal-organic frameworks: synthesis, stability and application in adsorption, CrystEngComm 14 (2012) 7099–7109.

[7] C.X. Yang, X.P. Yan, Metal-organic framework MIL-101 (Cr) for high-performance liquid chromatographic separation of substituted aromatics, Anal. Chem. 83 (2011) 7144–7150.

[8] E. Ruijter, R.V.A. Orru, Multicomponent reactions-opportunities for the pharmaceutical industry, Drug Discov, Today Technol 10 (2013) 15–20.

[9] C.M.R. Volla, I. Atodiresei, M. Rueping, Catalytic C-C bond-forming multi-component cascade or domino reactions: pushing the boundaries of complexity in asymmetric organocatalysis, Chem. Rev. 114 (2014) 2390–2431.

[10] H.A. Younus, M. Al-Rashida, A. Hameed, M. Uroos, U. Salar, S. Rana, K.M. Khan, Multicomponent reactions (MCR) in medicinal chemistry: a patent review (2010-2020), Expert Opin. Ther. Pat. 31 (2021) 267–289.

[11] J. Luo, G.S. Chen, S.J. Chen, Z.D. Li, Y.L. Liu, Catalytic enantioselective isocyanide-based reactions: beyond passerini and ugi multicomponent reactions, Chem. Eur J. 27 (2021) 6598–6619.

[12] M. Zhang, Y.H. Liu, Z.R. Shang, H.C. Hu, Z.H. Zhang, Supported molybdenum on graphene oxide/Fe_3O_4: an efficient, magnetically separable catalyst for one-pot construction of spiro-oxindole dihydropyridines in deep eutectic solvent under microwave irradiation, Catal. Commun. 88 (2017) 39–44.

[13] M.N. Chen, L.P. Mo, Z.S. Cui, Z. Zhang, Magnetic nanocatalysts: synthesis and application in multicomponent reactions, Curr. Opin. Green Sustain. Chem. 15 (2019) 27–37.

[14] L. Biesen, J.J. Muller, Multicomponent and one-pot syntheses of quinoxalines, Adv. Synth. Catal. 363 (2020) 980–1006.

[15] A. Chaudhary, Recent development in the synthesis of heterocycles by 2-naphthol-based multicomponent reactions, Mol. Divers. 25 (2021) 1211–1245.

[16] A.R. El-Gazzar, H. Hafez, Synthesis of 4-substituted pyrido-[2,3-d]pyrimidin-4(1H)-one as analgesic and anti-inflammatory agents, Bioorg. Med. Chem. Lett. 19 (2009) 3392–3397.

[17] M. Ghorab, F. Ragab, H. Heiba, R. Arafa, R.E. El-Hossary, In vitro anticancer screening and radiosensitizing evaluation of some new quinolines and pyrimido [4,5-b] quinolines bearing a sulfonamide moiety, Eur. J. Med. Chem. 45 (2010) 3677–3684.

[18] O. El-Sayed, H. Aboul-Enein, Synthesis and antimicrobial activity of novel pyrazolo [3,4-b]quinoline derivatives, Arch. Pharm. Pract. 334 (2001) 117–120.

[19] J. Quintela, C. Peinador, L. Botana, M. Estévez, R. Riguera, Synthesis and antihistaminic activity of 2-guanadino-3- cyanopyridines and pyrido[2,3-d]-pyrimidines, Bioorg. Med. Chem. 5 (1997) 1543–1553.

[20] S.R. Kanth, G.V. Reddy, K.H. Kishore, P.S. Rao, B.N. Murthy Usn, Convenient synthesis of novel 4-substitutedamino-5-trifluoromethyl–2,7-disubstituted pyrido [2,3-d]- pyrimidines and their antibacterial activity, Eur. J. Med. Chem. 41 (2006) 1011–1016.

[21] L.R. Bennett, C.J. Blankley, R.W. Fleming, R.D. Smith, D.K. Tessman, Antihypertensive activity of 6-arylpyrido [2,3-d]pyrimidin-7-amine derivatives, J. Med. Chem. 24 (1981) 382–389.

[22] S.J. Ji, S.N. Ni, F. Yang, J.W. Shi, G.L. Dou, X.Y. Li, D.Q. Shi, An Efficient synthesis of pyrimido[4,5-b]quinoline and indeno[2′,1′:5,6]pyrido[2,3-d]pyrimidine derivatives via multicomponent reactions in ionic liquid, J. Heterocycl. Chem. 45 (2008) 693–702.

[23] J.M. Khurana, A. Chaudhary, B. Nand, A. Lumb, Aqua mediated indium(III) chloride catalyzed synthesis of fused pyrimidines and pyrazoles, Tetrahedron Lett. 53 (2012) 3018–3022.

[24] B. Mirhosseini-Eshkevari, M.A. Ghasemzadeh, M. Esnaashari, S. Taghvaei Ganjali, Hexamethylenetetramine-based ionic liquid/MIL-101(Cr) metal-organic framework composite: a novel and versatile tool for the preparation of pyrido[2,3-d:5,6-d′] dipyrimidines, RSC Adv. 11 (2021) 364–373.

[25] M.A. Ghasemzadeh, M. Azimi-Nasrabad, S. Farhadi, B. Mirhosseini-Eshkevari, A highly efficient synthesis of 2, 4-diamino-6-arylpyrimidine-5-carbonitrile derivatives using NiCo2O4@Ni(BDC) metal-organic frameworks as a novel and bifunctional catalyst, J. Organomet. Chem. 900 (2019) 120935–120941.

[26] M.A. Ghasemzadeh, B. Mirhosseini-Eshkevari, M.H. Abdollahi-Basr, MIL-53(Fe) metal-organic frameworks (MOFs) as an efficient and reusable catalyst for the one-pot four-component synthesis of pyrano[2,3-c]-pyrazoles, Appl. Organomet. Chem. 33 (2018) 4679–4687.

[27] M.H. Abdollahi-Basir, F. Shirini, H. Tajik, M.A. Ghasemzadeh, Zn (BDC)-(MOF): introduction of a new catalyst for the synthesis pyrimido[4,5-d]Pyrimidine derivatives under ultrasound irradiation in the absence of solvent, Polycycl. Aromat. Comp. 41 (2019) 1580–1589.

[28] M.A. Ghasemzadeh, B. Mirhosseini-Eshkevari, M. Tavakoli, F. Zamani, Metal-organic frameworks: advanced tools for multicomponent reactions, Green Chem. 22 (2020) 7265–7300.

[29] T. Jin, Q. Yang, C. Meng, J. Xu, H. Liu, J. Hu, H. Ling, Promoting desulfurization capacity and separation efficiency simultaneously by the novel magnetic Fe_3O_4@PAA@MOF-199, RSC Adv. 4 (2014) 41902–41909.

[30] B. Mirhosseini-Eshkevari, M.A. Ghasemzadeh, J. Safaei-Ghomi, An efficient and green one-pot synthesis of indazolo [1,2-b]-phthalazinetriones via three-component reaction of aldehydes, dimedone, and phthalhydrazide using Fe3O4@SiO2 core-shell nanoparticles, Res. Chem. Intermed. 41 (2014) 7703–7714.

[31] S. Rostamnia, H. Alamgholiloo, M. Jafari, Ethylene diamine post-synthesis modification on open metal site Cr-MOF to access efficient bifunctional catalyst for the Hantzsch condensation reaction, Appl. Organomet. Chem. 32 (2018) e4370–e4378.

[32] Q. He, J. Liu, J. Liang, X. Liu, D. Tuo, W. Li, Chemically surface tunable solubility parameter for controllable drug delivery-an example and perspective from hollow PAA-coated magnetite nanoparticles with R6G model drug, Materials 11 (2018) 247–262.

[33] S. Salamat, H. Younesi, N. Bahramifar, Synthesis of magnetic core-shell Fe_3O_4@TiO_2 nanoparticles from electric arc furnace dust for photocatalytic degradation of steel mill wastewater, RSC Adv. 7 (2017) 19391–19405.

[34] P. Long, H. Wu, Q. Zhao, Y. Wang, J. Dong, Solvent effect on the synthesis of MIL-96 (Cr) and MIL-100 (Cr), Microporous Mesoporous Mater. 142 (2011) 489–493.

[35] M.M.A. Ghasemzadeh, J. Safaei-Ghomi, H. Molaei, Fe_3O_4 nanoparticles: as an efficient, green and magnetically reusable catalyst for the one-pot synthesis of 1,8-dioxo-decahydroacridine derivatives under solvent-free conditions, C. R. Chim. 15 (2012) 969–974.

[36] M. Mamaghani, F. Shirini, E. Bassereh, R. Hossein Nia, 1,2-Dimethyl-N-butanesulfonic acid imidazolium hydrogen sulfate as efficient ionic liquid catalyst in the synthesis of indeno fused pyrido[2,3-d]pyrimidines, J. Saudi Chem. Soc. 20 (2014) 570–576.

[37] F. Nemati, R. Saeedirad, Nano-Fe_3O_4 encapsulated-silica particles bearing sulfonic acid groups as a magnetically separable catalyst for green and efficient synthesis of functionalized pyrimido[4,5-b]quinolines and indeno fused pyrido[2,3-d] pyrimidines in water, Chin. Chem. Lett. 24 (2013) 370–372.

[38] F. Osanlou, F. Nemati, S. Sabaqian, An eco-friendly and magnetized biopolymer cellulose-based heterogeneous acid catalyst for facile synthesis of functionalized pyrimido[4,5-b]-quinolines and indeno fused pyrido[2,3-d]pyrimidines in water, Res. Chem. Intermed. 43 (2017) 2159–2174.

[39] J. Park, K. An, Y. Hwang, J.G, Park.H.J. Noh, J.Y, J.H. Kim, N.M. Park, T. Hyeon Hwang, Ultra-large-scale syntheses of monodisperse nanocrystals, Nat. Mater. 3 (2004) 891–895.

[40] M. Aguirre-Díaz, L. Gándara, F. Iglesias, M. Snejko, N. Gutiérrez-Puebla, E. Ángeles Monge, Tunable catalytic activity of solid solution metal-organic frameworks in one-pot multicomponent reactions, J. Am. Chem. Soc. 137 (2015) 6132, 1635.